Abrupt loss and uncertain recovery from fires of Amazon forests under low climate mitigation scenarios

Isabel Martínez Cano[a,1] 🆔, Elena Shevliakova[b], Sergey Malyshev[b], Jasmin G. John[b,c] 🆔, Yan Yu[d], Benjamin Smith[e,f] 🆔, and Stephen W. Pacala[a]

Tropical forests contribute a major sink for anthropogenic carbon emissions essential to slowing down the buildup of atmospheric CO_2 and buffering climate change impacts. However, the response of tropical forests to more frequent weather extremes and long-recovery disturbances like fires remains uncertain. Analyses of field data and ecological theory raise concerns about the possibility of the Amazon crossing a tipping point leading to catastrophic tropical forest loss. In contrast, climate models consistently project an enhanced tropical sink. Here, we show a heterogeneous response of Amazonian carbon stocks in GFDL-ESM4.1, an Earth System Model (ESM) featuring dynamic disturbances and height-structured tree–grass competition. Enhanced productivity due to CO_2 fertilization promotes increases in forest biomass that, under low emission scenarios, last until the end of the century. Under high emissions, positive trends reverse after 2060, when simulated fires prompt forest loss that results in a 40% decline in tropical forest biomass by 2100. Projected fires occur under dry conditions associated with El Niño Southern Oscillation and the Atlantic Multidecadal Oscillation, a response observed under current climate conditions, but exacerbated by an overall decline in precipitation. Following the initial disturbance, grassland dominance promotes recurrent fires and tree competitive exclusion, which prevents forest recovery. EC-Earth3-Veg, an ESM with a dynamic vegetation model of similar complexity, projected comparable wildfire forest loss under high emissions but faster postfire recovery rates. Our results reveal the importance of complex nonlinear responses to assessing climate change impacts and the urgent need to research postfire recovery and its representation in ESMs.

tropical forest | wildfires | forest recovery | earth system model

Tropical forests are a major reservoir of biodiversity that contribute key ecosystem services to the regulation of Earth's climate and carbon cycle. Recent studies raise concerns about the ability of tropical forests to sustain these services in the face of global change. For example, forest inventories provide direct evidence of a slowing sink in intact tropical forests (1, 2). This trend may be further aggravated in areas affected by land degradation, deforestation, and long-recovery disturbances associated with the increased frequency of weather extremes (3). The widespread and intense droughts observed in South America in recent years—2005, 2010, and 2015 to 2016—sparked severe, primarily intentional fires associated with land management (4) that burned millions of hectares of primary forests in the drier portions of the Amazon Basin and released vast amounts of CO_2 to the atmosphere (5–7). It is unclear whether such extreme disturbances represent an actual threat to the resilience of tropical forests, but they add to growing concerns about the possibility of a tipping point for the Amazon system (8) beyond which the remaining forest would dry out, turning forest to savanna (9).

The literature on Amazonian tipping points is in disagreement, with alternative bodies of evidence making opposite predictions. Empirical relationships between annual rainfall and vegetation type (forest vs. savanna vs. grassland) and simple models of tree–grass competition and fire suggest that tree vs. grass cover represents alternative stable states (10, 11). Savanna grasses favor the occurrence of fires by retaining highly flammable erect leaves and stems through the dry season (rather than their abscission) (12). Fire kills tree saplings that would eventually overtop the grasses and prevents competitive exclusion. Trees are much less flammable and decrease the likelihood of fires, granting saplings the time needed to replace trees that die and to fill gaps in the forest canopy. However, in an extremely dry year, forest patches can burn and rapidly convert to grassland, and a string of unusually wet years can allow saplings to overtop grasses and slowly convert savanna back to forest (13) (Fig. 1). These ecological mechanisms anticipate the possibility of a tipping point in the near future—a large loss of up to 20 to 40% of tropical forest (14) under rainfall regimes projected by climate models. Regional ecosystem–fire models further stress how drought-induced fires threaten the stability of Amazon forests (15), and how fragmentation and changes in land use might enhance the impact of fires under future

Significance

Assessments of alternative mitigation strategies to limit the impact of global change increasingly rely on simulations of Earth System Models (ESMs). In the tropics, a major biodiversity refuge and a net sink for anthropogenic carbondioxide emissions, ESMs consistently project that forests will thrive through the century due to enhanced plant photosynthesis. Using an ESM that accounts for the simultaneous effect of fires, water stress, and plant competition, we found that up to 40% of Amazon forests may begin to convert to savanna before mid-century under high emission scenarios. These results point to reassessing the resilience of tropical forests to climate-induced disturbances and urge action to reduce carbon emissions to prevent tropical forest degradation.

drier conditions (16). However, these projections do not account for physiological factors such as CO_2 fertilization that may benefit trees and prevent a tropical-forest tipping point.

Modern Earth System Models (ESMs), which include CO_2 fertilization and climate–vegetation feedbacks often missing from ecological models, come to the opposite conclusion. Although the first comprehensive ESM with dynamic vegetation projected large-scale dieback of the Amazon under rapid climate warming (17), recent ESMs consistently projected that tropical forests will thrive through the century (18, 19), maintaining both the "natural" tropical carbon sink and the viability of emission reduction initiatives based on reforestation [e.g., the Bonn Challenge (20)]. However, the computational burden of simulating coupled global climate and the carbon cycle often results in the adoption of a relatively simple representation of land vegetation (21). These ESMs do not include the ecological mechanisms responsible for the tipping point predicted by the ecological literature, but increasingly do project the drying that causes it, particularly in the Amazon (22–24).

In this paper, we bring these two bodies of work together by analyzing an ESM that includes the mechanisms present in both the alarming ecological literature (e.g., height-structured plant competition, grass fire feedbacks, and tree shade–fire suppression) and the reassuring climatological literature (CO_2 fertilization and large-scale climate–vegetation feedbacks; see also Fig. 1). Specifically, we analyze recent trends and future projections of tropical forest biomass and fire carbon emissions using GFDL-ESM4.1 (25), a fully coupled global climate and carbon cycle model contributing to Phase 6 of the Coupled Model Intercomparison Project (CMIP6) (26). The terrestrial biosphere component of GFDL-ESM4.1 (LM4.1) simulates vegetation dynamics by following the fate of individual demographic cohorts of multiple, competing vegetation types (27), including tropical trees and grasses. Realistic patch dynamics emerge through the simulation of multiple tiles within each ESM grid cell and subgrid scale disturbances like fires (28, 29). The outcome of height-structured competition among vegetation types and fires results in a mosaic of patches (tiles) with a varying degree of tree dominance, ranging from pure grasslands to forests through savanna landscapes. We focused on the response of tropical vegetation during global simulations for the 21st century under the low- and high-end emission forcing from the plausible Shared Socioeconomic Pathways (30) (SSP1-2.6 and SSP5-8.5, respectively) and briefly comment on results for intermediate emission scenarios. We first examined divergent responses in projected trends of tropical vegetation biomass across biogeographical realms. We analyzed the role of climate-induced fires as a driver of projected declines in the Amazon under high emissions. Finally, we used both the present-day observations and simulation results to assess the robustness of GFDL-ESM4.1 projections. We analyzed the subset of CMIP6 ESMs featuring dynamic vegetation and fires, conducting a more detailed comparison of ESM4.1 and EC-Earth3-Veg (31) projections, the two ESMs implementing complex vegetation dynamics.
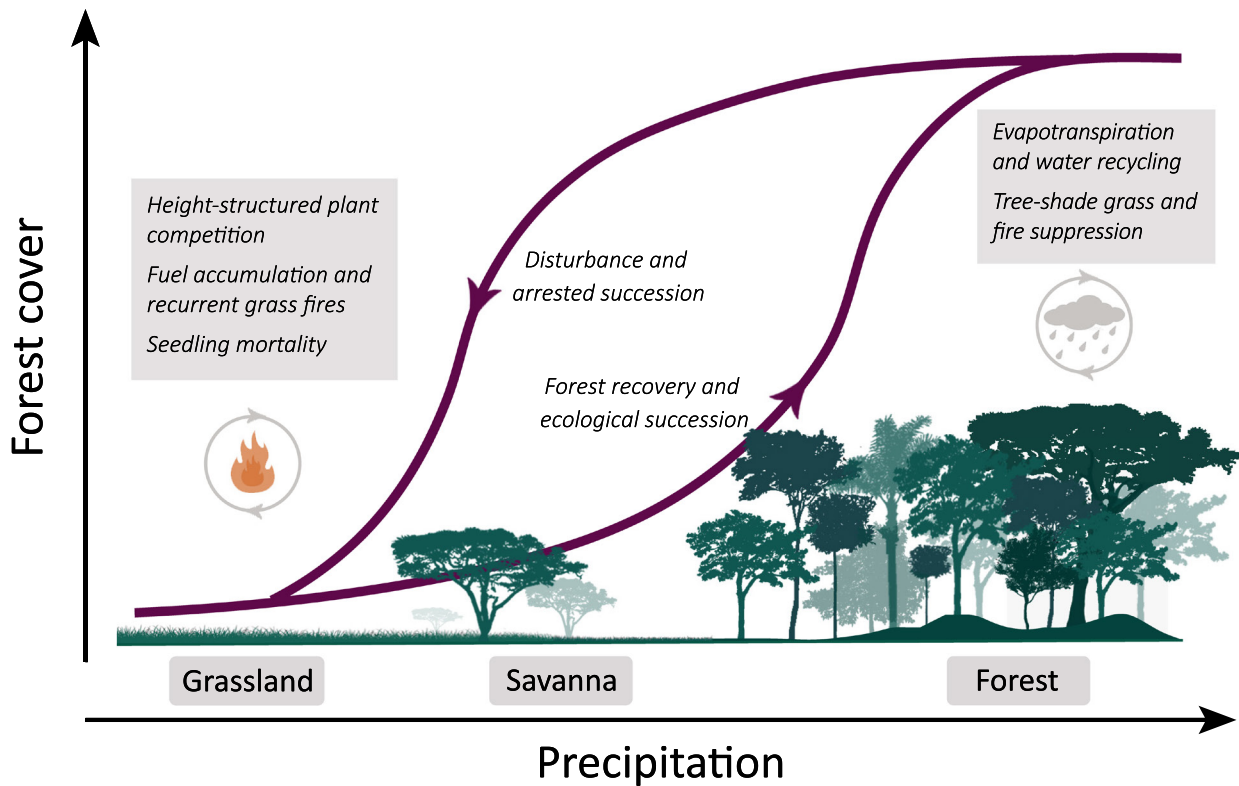
Fig. 1. Emergence of alternative states and hysteresis in the structure of tropical vegetation along a gradient of water availability. The schematic highlights key mechanisms implemented in the dynamic land model LM4.1 embedded in GFDL-ESM4.1. Low precipitation regimes favor the dominance of grasslands and savannas where seasonal fuel accumulation promotes recurrent fires that keep a state of arrested succession. High precipitation regimes converge toward a high tree cover state where the closed tree canopy inhibits grasses, reduces evaporative water loss, and increases transpiration to enhance moisture recycling at regional scales. Fire and humidity feedback mechanisms reinforce the resilience of each state and result in their coexistence at intermediate precipitation levels, where the dominant formation becomes contingent to past conditions. After a string of wet years, trees may be able to displace grasses, form a closed canopy, and reach a new alternative equilibrium. As conditions become drier, a closed forest canopy resiliently keeps humidity and prevents its own collapse until disturbances like fires prompt an abrupt transition to the low cover state.

Results

Projected Changes in Tropical Tree Biomass. GFDL-ESM4.1 simulates a distinct response of forest carbon stocks across the tropical biome and among climate change scenarios. The model concurs with observations in predicting a larger forest biomass in the Paleotropics (tropical areas of Africa and Asia) than in the Neotropics (tropical Americas) under current climate conditions (22.1 vs. 18.8 kg C m^{-2}, Fig. 2A and *SI Appendix*, Fig. S1). Projection experiments suggest that climate change will exacerbate regional differences in tropical forest biomass. GFDL-ESM4.1 projects an increase of forest biomass in the Paleotropics of 0.27 and 0.48 (% per year) under scenarios SSP1-2.6 and SSP5-8.5, respectively. At the same time, there is a diverging response to greenhouse gas (GHG) forcing in the Neotropics. Forest biomass increases steadily but at a slower pace under SSP1-2.6 (0.17% per year), a trend paralleled under the high emissions SSP5-8.5 until 2060, when biomass suddenly starts to decay to levels 40% below the initial stock (*SI Appendix*, Fig. S1A). Experiments run under intermediate scenarios resulted in similar qualitative trends to those projected for the low- and high-end scenarios; GFDL-ESM4.1 projects a smooth increase in tree biomass under SSP2-4.5, but rapid forest decline after 2080 under scenario SSP3-7.0 (*SI Appendix*, Fig. S2).

Examination of tree biomass trajectories at individual grid cells dominated by forests at the start of the simulation reveals a heterogeneous response under SSP5-8.5 (Fig. 2B). Some cells feature local increases in tree biomass that remain consistent with the positive effect of CO_2 fertilization on photosynthesis. On the contrary, fires caused declines in tree biomass in half of the grid cells, leading to biomasses below 5 kg C m^{-2} (32%) in the Amazonia by the end of the simulation (Fig. 2B and *SI Appendix*, Figs. S3 and S4). This heterogeneous response occurs at intermediate precipitation levels where either savannas or forests dominate the present-day tropical landscapes (11), suggesting an emergent

transition between alternative stable states in GFDL-ESM4.1 (Fig. 2C and *SI Appendix*, Fig. S5).

Drivers of Projected Natural Fires in the Amazon. The occurrence and impact of nonagricultural fires in GFDL-ESM4.1 is an emergent process modulated by a set of interacting factors that depend on meteorological conditions, human population density, and vegetation status and functioning (28). Analyzing projected trends in these factors revealed that decreases in soil moisture and relative humidity prompted the increased prevalence of forest fires in the Amazon under SSP5-8.5 (*SI Appendix*, Fig. S6). These trends parallel the decline in precipitation in the Amazon projected by GFDL-ESM4.1, which falls close to the ensemble mean of CMIP6 ESMs (22–24) (n = 21, *SI Appendix*, Figs. S7–S9). In the first years of the projection experiment, humid conditions prevailed during the entire year, buffering against the occurrence of fires (Fig. 3). As the simulation progressed, decreases in soil moisture and relative humidity during the dry season became more extreme. The sequence involves the depletion of soil moisture through evapotranspiration, a process which in a normal year contributes to keep humid conditions within the canopy. However, reduced water storage and enhanced water stress during low precipitation years with prolonged dry seasons exhausted the buffering mechanism and triggered a sudden amplification of forest fires after 2060 under SSP5-8.5 (Fig. 4).

Assessment of Simulated Fires. The possibility of abrupt responses under increasingly dry conditions rests on the mechanistic representation of fires in GFDL-ESM4.1. Simulated fires mimic observed, large-scale gradients in the distribution, intensity, and seasonality of fires detected by satellites across the tropics during the last two decades (*SI Appendix*, Figs. S10–S15). Like other CMIP6 models, GFDL-ESM4.1 tends however to overestimate fire intensity and extent along biome boundaries and in tropical regions with high cloud cover, biases that remain consistent with
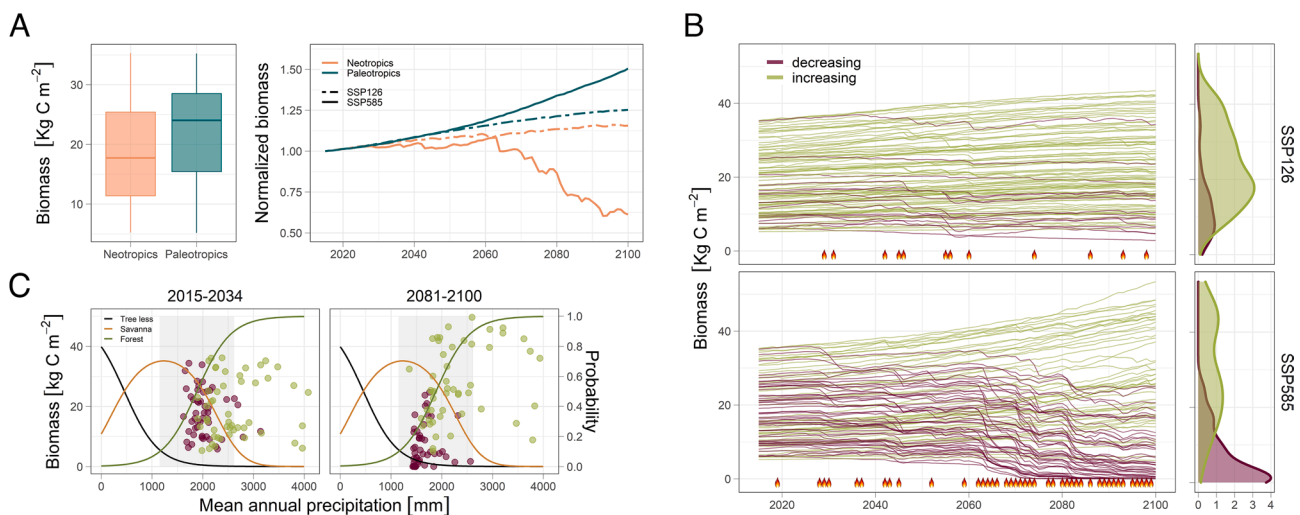
Fig. 2. (*A*) *Left*: Distribution of total tree biomass in the Neotropics and in the Paleotropics at the end of GFDL-ESM4.1 simulations during the historical period (the boxplots show the median and central interquartile range). *Right*: Projected trends in biomass under scenarios SSP1-2.6 and SSP5-8.5 (values normalized to the initial stock). (*B*) Projected trends in total tree biomass in the Neotropics based on GFDL-ESM4.1 global simulations under CMIP6 emission scenarios SSP1-2.6 and SSP5-8.5. Each line corresponds to the dynamics of natural tropical forests in an individual grid cell location (i.e., tiles that were unaffected by changes in land use). Trajectories showing a decrease in total biomass are highlighted with a purple hue. Flames along the abscissa indicate years with high carbon emissions due to fires. The complementary *SI Appendix*, Fig. S4 highlights the relationship between trends in tree biomass and changes in precipitation. *Right*: Distribution (as probability density function) of tree biomass by the end of the simulation for grid cell locations showing increasing or decreasing trends. (*C*) Relationship between tree biomass and mean annual precipitation (MAP, mm) at the start (2015 to 2034) and at the end (2081 to 2100) of simulations under scenario SSP5-8.5. The reference lines represent the probability of different vegetation types (treeless, savanna, and forest) estimated by ref. 11 based on remote sensing observations of vegetation cover and precipitation over South America. The background gray area delimits a bistability zone where the probability that forest is the dominant vegetation type is between 0.1 and 0.9. *SI Appendix*, Fig. S5 depicts the trajectories of each grid cell on tree biomass-MAP coordinates.
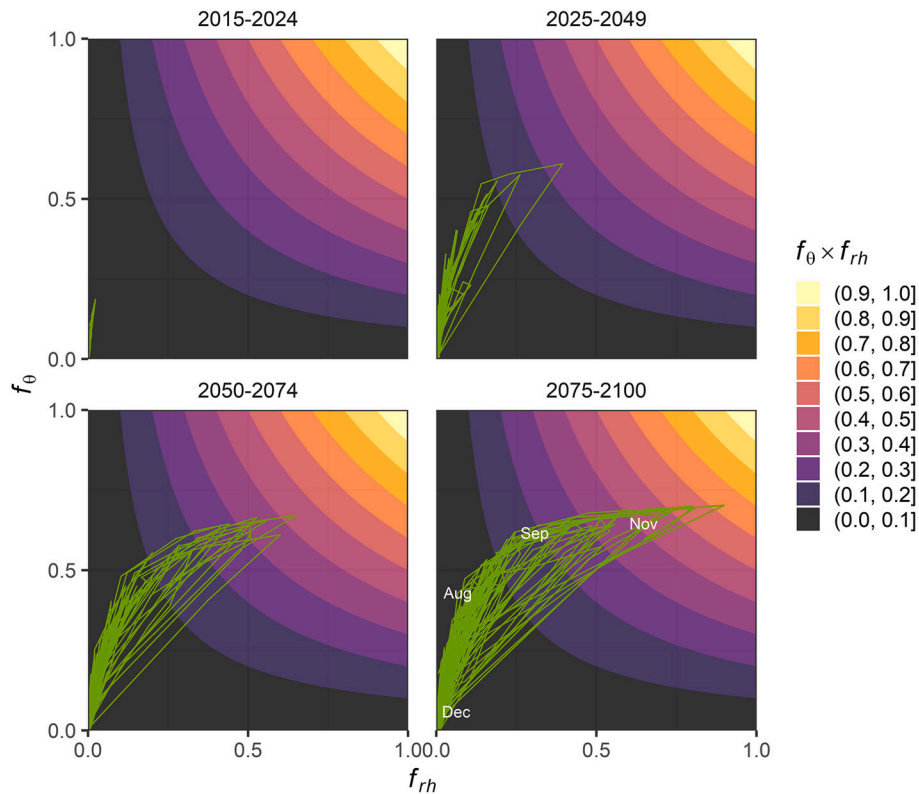
Fig. 3. Seasonal changes in GFDL-ESM4.1 fire suppression factors for soil moisture (f_θ) and relative humidity (f_{rh}) under scenario SSP5-8.5 for a representative grid cell located in the Amazon. Each panel corresponds to a different period during the simulation and the green paths show the seasonal cycle of f_θ and f_{rh} during each year. The background color provides the combined effect of both factors on fire probability; i.e., as the green path moves toward the *Upper Right* corner of each panel, fires become more likely. See *SI Appendix* for details on the fire suppression factors.

the known limitations of satellites to detect small fires (32, 33). In the Neotropics, remote climate forcing associated with El Niño Southern Oscillation (ENSO) and Atlantic Multidecadal Oscillation (AMO) can be used to forecast the number of fires during the dry season (34), providing a mechanistic link to diagnose the reliability of fires in GFDL-ESM4.1. Except in areas with large biases in simulated precipitation (i.e., the Guiana shield), GFDL-ESM4.1 historical simulations exhibit the positive correlation between the Oceanic Niño Index (ONI) and interannual fire emissions observed over a great portion of the Amazon basin, especially in the northeast, as well as the greater influence of AMO on fire activity in the southern Amazonia ($r > 0.7$ in both cases, Fig. 4). These patterns are not reproduced by other CMIP6 models (*SI Appendix,* Figs. S16–S18). ESM projections concur in that ENSO events are becoming more intense with global warming (35, 36), a trend that indirectly suggests an increased likelihood of dry conditions favoring fire activity in the Amazon.

Projected Responses of Tropical Vegetation in CMIP6 ESMs. The emergence of abrupt responses to external forcing is a desirable, albeit rarely documented feature of ESMs. The timing and emergence of tipping points in ESMs remains highly uncertain (37), and previous assessments reported a low likelihood of abrupt change in the Amazon during this century (18, 38). We analyzed the output of the subset of CMIP6 models with dynamic vegetation and fires ($n = 6$, *SI Appendix,* Table S1) to determine whether other ESMs project potential forest losses due to fires in the period to year 2100. Although most models projected an increase in Amazon forest biomass during the 21st century under SSP5-8.5, the response to fires and GHG emissions varied depending on the complexity of their vegetation modules. ESMs

with less sophisticated vegetation dynamics simulated a fairly homogenous response, with forests growing at a constant pace that resulted in a steady increase in biomass (~0.05% per year, Fig. 5 and *SI Appendix,* Fig. S19). On the contrary, the two ESMs featuring complex vegetation processes—GFDL-ESM4.1 and EC-Earth3-Veg (31, 39)—simulated a more heterogeneous response, with huge losses due to fires and periods of fast vegetation growth.

Both GFDL-ESM4.1 and EC-Earth3-Veg simulated comparable biomass losses due to fires (23.4 vs. 22.5% of years decreasing at similar rates, Fig. 5). However, rates of biomass change when biomass was increasing in EC-Earth3-Veg almost doubled those in GFDL-ESM4.1 at low biomass levels, and they tended to be faster than rates simulated by other CMIP6 ESMs (Fig. 5 and *SI Appendix,* Figs. S19–S21). As a consequence, the projected net change in biomass between 2015 and 2100 differs between these two models; repeated fires drag toward a regional decline in forest biomass in GFDL-ESM4.1, while the faster rates of biomass increase in EC-Earth3-Veg ultimately result in a net increase in biomass (*SI Appendix,* Fig. S22). Differences in simulated water availability might determine the failure of recently burned forest areas to recover following fires of similar magnitude. However, rates of biomass increase remain larger in EC-Earth3-Veg than that in GFDL-ESM4.1 even under similar meteorological conditions. To rule out that differences between the two models emerged from potential biases in the simulation of precipitation extremes, we performed a dedicated experiment forcing GFDL-ESM4.1 with sea surface temperature fields simulated by EC-Earth3-Veg to resemble its climate teleconnection patterns (i.e., the remote effects of ENSO and AMO). Such simulations resulted in abrupt forest loss (*SI Appendix,* Fig. S24), evidencing that underlying
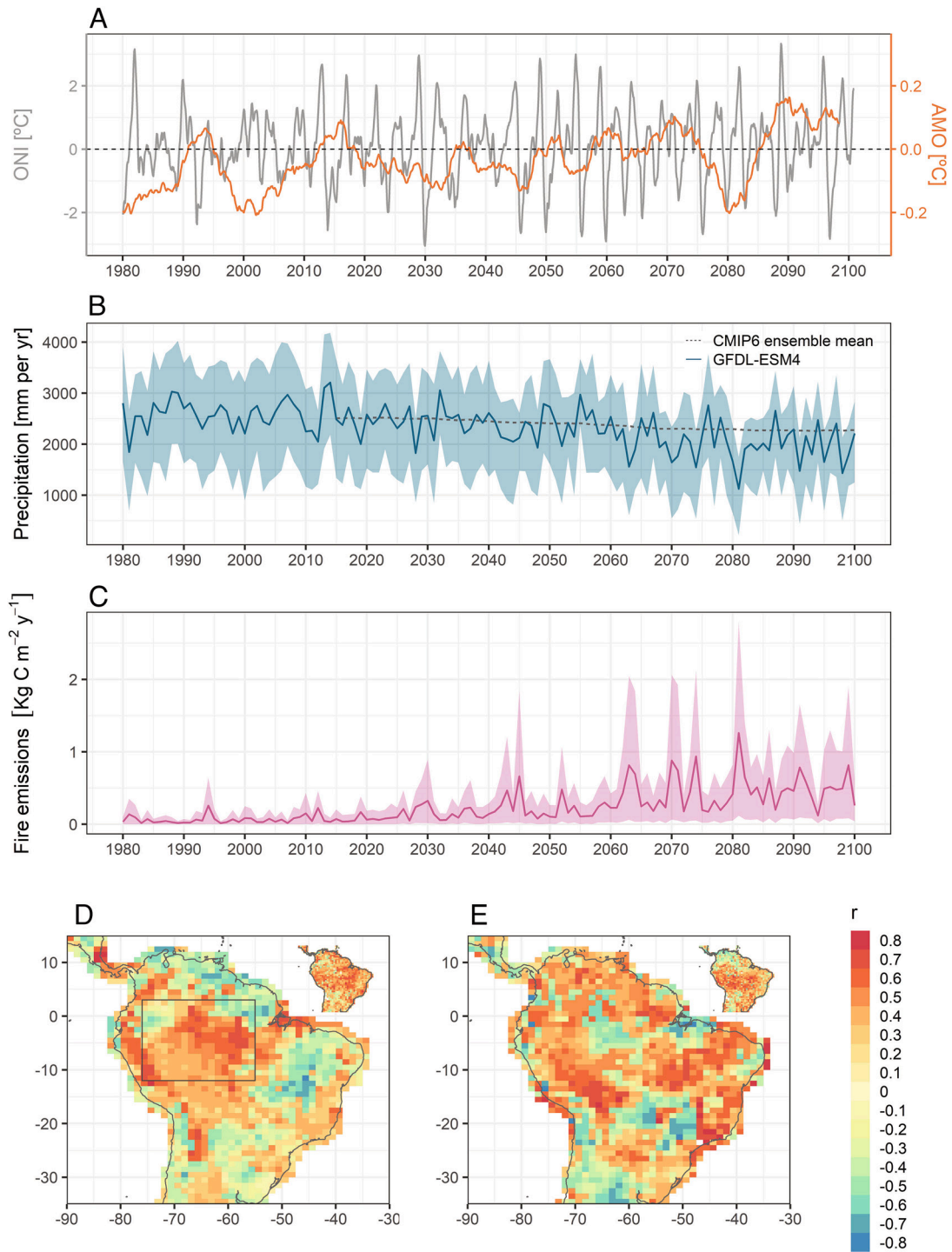
Fig. 4. (A–C) Time series combining GFDL-ESM4.1 historical (1980 to 2014) and SSP5-8.5 (2015 to 2100) simulations for (A) the ONI (°C) and the AMO (°C), and (B) precipitation during the dry season (October–March, mm y^{-1}; the dashed line shows the ensemble mean across n = 21 CMIP6 ESMs, see *SI Appendix*, Table S2), and (C) the rate of release of carbon lost through fires to the atmosphere (fire carbon emissions, kg C m^{-2} y^{-1}) averaged (mean and 80%CI) over the Amazon. (D and E) Maps of the maximum absolute correlation coefficient r between annual changes in fire carbon emissions and lagged values of (D) ONI and (E) AMO climate teleconnection indices. The box in (D) limits the area used to summarize time series data presented in panels (B and C). *Insets* provide reference maps based on remote sensing observations (1997 to 2014). See *SI Appendix*, Table S1 and Figs. S10–S18 for additional information about the simulation of fires in GFDL-ESM4.1 and in other CMIP6 ESMs.

differences on the representation of vegetation dynamics and hydrological processes account for diverging forest responses between the two models under high-emission scenarios (*SI Appendix*, Table S1 and Supplementary Text). Together, these results point to highly uncertain postfire recovery dynamics as a key process to explain differences among model projections.

Discussion

Despite fires implicitly contributing to prescribed deforestation in SSP experimental protocols, most ESMs still ignore drought-related fire disturbance and lack a detailed representation of the lasting impact of fires. The paucity of ESMs featuring fires and
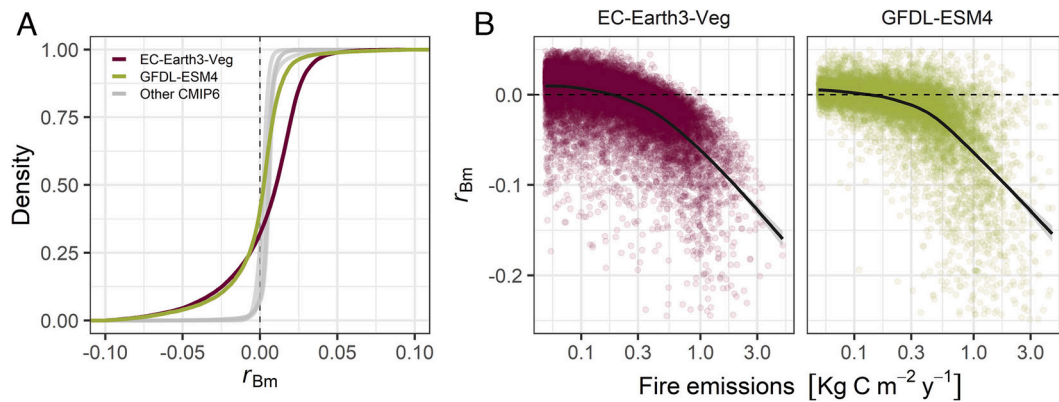
Fig. 5. Distribution of the relative rates of biomass increase (r_{Bm}, y^{-1}) simulated by GFDL-ESM4.1, EC-Earth3-Veg, and other CMIP6 ESMs (CESM2, CNRM-ESM2-1, MRI-ESM2-0, and NorESM2-LM; see *SI Appendix*, Table S1 for further details) under scenario SSP5-8.5. Relative rates were calculated as the natural logarithm of the ratio of annual woody biomass between consecutive years during the period 2015 to 2100. (*A*) Empirical cumulative distribution function of simulated r_{Bm}. (*B*) Relationship between r_{Bm} and carbon emissions to the atmosphere due to fires (fire emissions, kg C m^{-2} y^{-1}) in EC-Earth3-Veg and GFDL-ESM4.1 models.

complex vegetation dynamics prevents the identification of emergent constraints to reduce uncertainty in tropical forest responses to climate change (40). Most models project a widespread increase in forest biomass and suggest that the positive effect of CO_2 fertilization will prevail over vegetation losses under warmer and drier conditions, including EC-Earth3-Veg, one of the ESMs featuring patch dynamics and size-structured vegetation dynamics. The other model incorporating complex vegetation processes, GFDL-ESM4, simulates a more heterogeneous response (41) in which forest biomass may decline in drier areas. ESMs lacking patch dynamics implement a partial decrease in biomass following fires that leave an unaltered forest tree size structure, obviating feedback mechanisms that might hinder forest recovery (4). In GFDL-ESM4.1, fires affecting large areas trigger the formation of disturbed patches with reduced tree dominance to resemble fire scars and their recovery after the disturbance. Lower canopy height and reduced forest cover favor the competition with other vegetation types (i.e., highly flammable C_3 and C_4 grasses) and increase water stress by reducing moisture recycling in recently burned patches, resulting in an easily dried and fuel-laden forest. These conditions hinder tree growth and can even lead to recurrent fires that keep the forest in a state of arrested recovery with low tree cover and an abundant grass layer that resembles a savanna landscape, as projected for drier areas in SSP5-8.5 (*SI Appendix*, Fig. S25). Importantly, EC-Earth3-Veg simulated a comparable impact of wildfires on tropical vegetation, but it also projected that forest will nonetheless thrive under high emissions due to a higher resilience and faster pace of forest recovery.

As the dominance of tropical landscapes by secondary forests and treeless formations grows due to forest degradation and deforestation (42, 43), understanding the interaction of forest management with the dynamics of disturbance and successional recovery turns into an urgent need (14). Here, we found that climate-induced tree mortality due to fires might become a key driver of forest damage in the Amazon during this century, prompting the inclusion of fire disturbances and height-structured competition in ESMs. Uncertainties about the incidence of fires in tropical areas (33) further highlight the need of continued efforts to jointly improve ESM projections and satellite products. While the prevalence of fires also depends on highly uncertain projections of future precipitation and drought regimes, GFDL-ESM4.1 fires are consistent with known climate teleconnection drivers and CMIP6 ESMs robustly project drier conditions in the Amazon (22–24). However, ESMs predicting similar fires do not

project comparable forest losses, including EC-Earth3-Veg, a model with complex vegetation dynamics, cautioning the need to further research postfire recovery and tree–grass interactions. Postfire recovery dynamics emerged as a major source of uncertainty of ESM projections of tropical vegetation dynamics. Another source of uncertainty arises from simplifying assumptions about the variety of vegetation types featured in most ESMs, which do not reflect the potential ability of compositional shifts (44) to buffer the impact of fires by favoring species with rapid growth or high bark thickness (45). Our findings align with growing concerns about the resilience of tropical forests arising from observed increases in tree mortality and the incipient saturation of the Amazon tropical sink despite CO_2 fertilization (1, 2) and warn about the potential contribution of meteorological extremes to advance the onset of abrupt transitions. As a consequence, our results call for mitigation initiatives to prevent fire-induced forest degradation and urge the adoption of low-emission policies to avoid further damaging of Amazon forest ecosystems.

Methods

Land Model in GFDL-ESM4.1. The land model LM4.1 improves the representation of ecological and plant physiological processes with respect to its antecessors (see *SI Appendix* for a description of key components of model). A key advance defining this model is the representation of vegetation dynamics using multiple competing cohorts arranged in canopy layers according to the Perfect Plasticity Approximation, PPA (46, 47). The model allows the formation of forest canopy gaps following a disturbance and represents landscape heterogeneity through the simulation of multiple coexisting tiles at different successional forest stages and distinct land uses within the same ESM grid cell. In addition, LM4.1 features a new plant hydraulics module (48) that combines constraints on carbon acquisition and hydraulic impairment that affect the survival of seedlings and understory plants. The model also features updated land-use routines, a prognostic dust emission model (49, 50), and a new state-of-the-art daily fire model, FINAL v2 (28, 29) (*SI Appendix*).

To implement tropical forest vegetation, LM4.1 incorporates a dedicated vegetation type resembling the traits of shade-tolerant tree species dominating the forest canopy at Barro Colorado Island (BCI, Panama). Simulations with prescribed reanalysis forcing data predicted carbon fluxes within the range of available estimates at BCI and captured diurnal and seasonal response variability in forest productivity. The model also captured first-order variability in individual growth rates between canopy and understory trees. Importantly, simulations at multiple locations also captured large-scale, spatial gradients in forest biomass and key emergent properties like variability in tree size structure across the tropics (27). In LM4.1, the distribution and abundance of tropical forests reflects the outcome

of competitive interactions with other vegetation types modulated by climatic constraints on physiological performance. The model simulates the dynamics of five vegetation types that compete among them for light and water (tropical, temperate, and conifer trees, and C3 and C4 grasses).

CMIP6 Experiments. Our core analyses focused on GFDL-ESM4.1 simulations developed as part of the CMIP6 (26). We retrieved the output of concentration-driven 21st-century experiments (2015–2100) under the two ends of the plausible SSPs, SSP1-2.6 and SSP5-8.5 (30). Scenario SSP1-2.6 represents the most benign future pathway, with radiative forcing increasing up to 2.6 W/m^2 in 2100 (similar to RCP2.6 global forcing pathway in CMIP5) and SSP1 socioeconomic conditions (policies favoring sustainability and low challenges to mitigation and adaptation). On the contrary, scenario SSP5-8.5 reaches 8.5 W/m^2 in 2100 (similar to RCP8.5) and features SSP5 socioeconomic conditions (fossil-fueled development with high challenges to mitigation and low challenges to adaptation).

We classified GFDL-ESM4.1 grid cells based on Köppen climate classification using monthly temperature and precipitation climatologies for the period 1951 to 1980. We selected those cells classified as tropical rainforest Köppen climate for further analyses. With respect to the use of a predefined window, this filtering step avoided prevailing biases in the simulation of precipitation over the tropics by ESMs (51). We focused on the projected dynamics of the biomass of natural tropical forests [i.e., tiles that were unaffected by changes in land use during the simulation and with an initial tree biomass above 5 kg C m^{-2}, a figure which provides a threshold to identify areas covered by forest (52)]. We also retrieved historical concentration-driven simulations (1980 to 2014) to assess model performance in relation to forest plot inventory data and fire products derived from remote sensing data (see below).

We complemented the analyses of GFDL-ESM4.1 with a comparative assessment of future trends in tropical carbon stocks in other ESMs contributing to CMIP6. We selected those models reporting trends in woody biomass (cWood) and fire diagnostics (fFire) over entire cells for scenario SSP5-8.5 ($n = 6$, see details in *SI Appendix*, Table S1). We retrieved time series of woody biomass at grid cells located in the Amazon and covered by forests, averaging experiments across multiple variant labels (ensembles), if available.

To assess the robustness of the projected decline in Amazon precipitation, we compared precipitation trends in a large subset of CMIP6 ESMs experiments under scenario SSP5-8.5 ($n = 21$, ESMs listed in *SI Appendix*, Table S2). We followed ref. (24) and analyzed changes in total precipitation over October–March in the Neotropics for the period 2015–2100.

Prescribed SST Simulation Experiment. We conducted a simulation experiment to test the sensitivity of abrupt forest losses observed in GFDL-ESM4.1 to potential biases in simulated weather conditions, especially precipitation extremes associated with sea surface temperature (SST) anomalies over the adjacent tropical oceans (i.e., remote effects of ENSO and AMO state). To do that, we forced GFDL-ESM4.1 atmosphere with the SST fields simulated by EC-Earth3-Veg model under scenario SSP5-8.5. As detailed in *SI Appendix*, Table S1, EC-Earth3-Veg implements dynamic vegetation and fires, but consistently projects a net increase in woody biomass between 2015 and 2100 (*SI Appendix*, Fig. S22). The experimental setup required adapting the resolution of some fields and the spatial extent of model domains (e.g., ts, siconca) in EC-Earth3-Veg to match GFDL-ESM4.1 specifications. The simulation experiment started from the state of GFDL-ESM4.1 at the end of CMIP6 historical period (2015-01-01) and continued under scenario SSP5-8.5 until the end of the century, using standard protocols and a dynamic atmosphere and land, but using EC-Earth3-Veg SST and sea ice concentration fields.

Fire and Climatic Data. To assess the ability of GFDL-ESM4.1 to reproduce the impact of natural fires on vegetation, we retrieved monthly, quarter degree resolution maps for the period 1997 to 2014 from the Global Fire Emissions Database, Version 4.1 (GFED4s, http://globalfiredata.org/index.html), a product based on Moderate Resolution Imaging Spectroradiometer (MODIS) images. We focused on two metrics characterizing the extent and intensity of natural fires: total burned area, which included small fires and that was converted to burned area fraction (53), and daily fire carbon emissions to the atmosphere, which were adjusted to an annual emission rate (54) (hereafter fire C emissions, kg C m^{-2} y^{-1}). The estimates provided by this product are conservative and tend to underestimate small fires (32).

We conservatively interpolated the original data to the model grid resolution and compared observed and simulated fires in a geographical and in a climate space (i.e., with coordinates defined in terms of mean annual precipitation and temperature). The latter approach complemented the assessment of fire extent and intensity to further examine whether GFDL-ESM4.1 fires occur under the right weather conditions. Monthly, one degree resolution temperature and precipitation maps for the period 1997 to 2014 were retrieved from Berkeley Earth reanalysis (http://berkeleyearth.org/data), and from NOAA Global Precipitation Climatology Center (GPCC, Total Full 552 V2018, https://psl.noaa.gov).

Climatic Indices. We analyzed the relationship between annual changes in carbon fire emissions in South America and two climate teleconnection indices: ONI and AMO. The analyses follow the approach in ref. (34), which established a predictive link to forecast the number of fires observed in the Amazon during the dry season based on ONI and AMO. We conducted the analyses both on ESM projections from the subset of CMIP6 ESMs with dynamic vegetation and fires (*SI Appendix*, Table S1) and on observational fire datasets (see above), which provided a benchmark to assess the reliability of simulated fires.

ONI was calculated from monthly time series of averaged sea surface temperature anomalies over the box [5°N-5°S, 120°W-170°W; Pacific Ocean]. We followed the methods of NOAA Climate Prediction Center and used a 30-y moving window to calculate SST seasonality (window updated for each pentad) and smoothed the resulting anomalies with a 3-mo moving average. AMO was calculated following ref.(55): monthly sea surface temperature anomalies were averaged over the box [75°W–7°W, 25°N–60°N; North Atlantic Ocean]. Then, to remove the trend due to anthropogenic climate change, we regressed the series against global sea surface temperature and retained the residuals, which were further smoothed using a 5-y moving average. See ref.(25) for an extensive assessment of climate variability in GFDL-ESM4.1 and ref.(36) for a comparative analysis of the CMIP6 ESM ensemble.

For each Neotropical grid cell, we determined the timing of the seasonal peak in fires over the historical period (*SI Appendix*, Fig. S15), which was calculated as the (circular) average month with the highest fire carbon emission. Then, we identified the optimal lag for each location based on the estimated correlation between annual fire carbon emission and each of the climate indices (ONI, AMO) lagged month by month up to 12 mo before the peak in fires. Finally, we modeled annual fire emissions as a linear combination of the two climate indices sampled during the month of maximum correlation:

$$C_{fire}(x, t) = a(x) + b(x) \times \text{ONI}(t, m(x) - \tau_{\text{ONI}}(x)) + c(x) \times \text{AMO}(t, m(x) - \tau_{\text{AMO}}(x)),$$

where x and t are location and year indices, respectively, $m(x)$ is the peak fire month at each location, and τ_{ONI} and τ_{AMO} are the optimal lag times for ONI and AMO, respectively.

Evaluation of Forest Biomass and Structure. We examine the ability of the model to reproduce i) large-scale gradients in forest biomass, ii) tree size distribution, and iii) trends in carbon gains in the tropics. We first compared Above Ground Biomass (AGB) reconstructions derived from forest plot estimates (56) across the tropics with GFDL-ESM4.1 estimates. Each forest plot was assigned to the nearest model grid cell to extract average biomass during the last 5 y of the historical simulation (2010 to 2014). AGB observations located in the same model grid cell were averaged before the analysis. Then, we assessed the ability of the model to reproduce forest size structure (i.e., the abundance of trees at different size classes). We retrieved data from BCI (http://ctfs.si.edu) forest plot to estimate the size spectrum after pooling data for all individuals recorded in the 2010 census.

Finally, we compared trends in carbon gains during the historical period in GFDL-ESM4.1 with the field estimates reported by refs. (1) and (2) for the Amazon. These authors reconstructed time series of the net carbon sink and the corresponding gains and losses based on estimates of tree growth, recruitment, and mortality from a large set of intact tropical forest census plots. To retrieve a comparable figure from GFDL-ESM4.1 output, we analyzed annual increases in the biomass of each cohort of the tropical tree vegetation type. As above, GFDL-ESM4.1 estimates are based on historical experiments ran with prescribed CO_2 levels. Note that GFDL-ESM4.1 is a free running model with interactive atmosphere, ocean, and land components. Thus, we expect GFDL-ESM4.1 to capture the long-term trends in the carbon gains, but to resemble high-frequency variability out of phase.

Author affiliations: aDepartment of Ecology and Evolutionary Biology, Princeton University, Princeton, NJ 08544; bNational Oceanic and Atmospheric Administration (NOAA)/Office of Oceanic and Atmospheric Research (OAR)/Geophysical Fluid Dynamics Laboratory, Princeton, NJ 08540; cNational Oceanic and Atmospheric Administration (NOAA)/Office of Oceanic and Atmospheric Research (OAR)/Atlantic Oceanographic and Meteorological Laboratory, Miami, FL 33149; dDepartment of Atmospheric and Oceanic Sciences, School of Physics, Peking University, 100084, China; eDepartment of Physical Geography and Ecosystem Science, Lund University, Lund 22100, Sweden; and fHawkesbury Institute for the Environment, Western Sydney University, Penrith, NSW 2751, Australia

1. R. J. W. Brienen *et al.*, Long-term decline of the Amazon carbon sink. *Nature* **519**, 344–348 (2015), 10.1038/nature14283.
2. W. Hubau, Asynchronous carbon sink saturation in African and Amazonian tropical forests. *Nature* **579**, 80–87 (2020), 10.1038/s41586-020-2035-0.
3. M. S. Morales *et al.*, Six hundred years of South American tree rings reveal an increase in severe hydroclimatic events since mid-20th century. *Proc. Natl. Acad. Sci. U.S.A.* **117**, 16816–16823 (2020), 10.1073/pnas.2002411117.
4. M. A. Cochrane, Fire science for rainforests. *Nature* **421**, 913–919 (2003), 10.1038/nature01437.
5. P. M. Brando *et al.*, Abrupt increases in Amazonian tree mortality due to drought-fire interactions. *Proc. Natl. Acad. Sci. U.S.A.* **111**, 6347–6352 (2014), 10.1073/pnas.1305499111.
6. A. A. Alencar, P. M. Brando, G. P. Asner, F. E. Putz, Landscape fragmentation, severe drought, and the new Amazon forest fire regime. *Ecol. Appl.* **25**, 1493–1505 (2015), 10.1890/14-1528.1.
7. K. Withey *et al.*, Quantifying immediate carbon emissions from El Nino-mediated wildfires in humid tropical forests. *Philos. Trans. R. Soc. B Biol. Sci.* **373**, 20170312 (2018), 10.1098/rstb.2017.0312.
8. T. E. Lovejoy, C. Nobre, Amazon tipping point: Last chance for action. *Sci. Adv.* **5**, eaba2949 (2019), 10.1126/sciadv.aba2949.
9. C. A. Nobre, P. J. Sellers, J. Shukla, Amazonian Deforestation and regional climate change. *J. Clim.* **4**, 957–988 (1991), 10.1175/1520-0442(1991)004<0957:ADARCC>2.0.CO;2.
10. A. C. Staver, S. Archibald, S. A. Levin, The global extent and determinants of savanna and forest as alternative biome states. *Science* **334**, 230 (2011), 10.1126/science.1210465.
11. M. Hirota, M. Holmgren, E. H. Van Nes, M. Scheffer, Global resilience of tropical forest and savanna to critical transitions. *Science* **334**, 232 (2011), 10.1126/science.1210657.
12. S. Archibald, G. P. Hempson, C. A. Lehmann, Unified framework for plant life-history strategies shaped by fire and herbivory. *New Phytol.* **224**, 1490–1503 (2019), 10.1111/nph.15986.
13. I. Oliveras, Y. Malhi, Many shades of green: The dynamic tropical forest-savannah transition zones. *Philos. Trans. R. Soc. B Biol. Sci.* **371**, 20150308 (2016), 10.1098/rstb.2015.0308.
14. C. A. Nobre *et al.*, Land-use and climate change risks in the Amazon and the need of a novel sustainable development paradigm. *Proc. Natl. Acad. Sci. U.S.A.* **113**, 10759 (2016), 10.1073/pnas.1605516113.
15. B. L. De Faria *et al.*, Current and future patterns of fire-induced forest degradation in Amazonia. *Environ. Res. Lett.* **12**, 095005 (2017), 10.1088/1748-9326/aa69ce.
16. P. M. Brando *et al.*, The gathering firestorm in southern Amazonia. *Sci. Adv.* **6**, eaay1632 (2020), 10.1126/sciadv.aay1632.
17. P. M. Cox *et al.*, Amazonian forest dieback under climate-carbon cycle projections for the 21st century. *Theor. Appl. Climatol.* **78**, 137–156 (2004), 10.1007/s00704-004-0049-4.
18. C. Huntingford *et al.*, Simulated resilience of tropical rainforests to CO2-induced climate change. *Nat. Geosci.* **6**, 268–273 (2013), 10.1038/ngeo1741.
19. A. Koch, W. Hubau, S. L. Lewis, Earth system models are not capturing present-day tropical forest carbon dynamics. *Earth's Future* **9**, e2020EF001874 (2021), 10.1029/2020EF001874.
20. United Nations Environment Programme (UNEP), *The Bonn Challenge* (2011), https://www.bonnchallenge.org/.
21. R. A. Fisher *et al.*, Vegetation demographics in Earth system models: A review of progress and priorities. *Global Change Biol.* **24**, 35–54 (2018), 10.1111/gcb.13910.
22. B. I. Cook *et al.*, Twenty-first century drought projections in the CMIP6 forcing scenarios. *Earth's Future* **8**, e2019EF001461 (2020), 10.1029/2019EF001461.
23. A. M. Ukkola, M. G. De Kauwe, M. L. Roderick, G. Abramowitz, A. J. Pitman, Robust future changes in meteorological drought in CMIP6 projections despite uncertainty in precipitation. *Geophys. Res. Lett.* **47**, e2020GL087820 (2020), 10.1029/2020GL087820.
24. L. A. Parsons, Implications of CMIOP6 projected drying trends for 21st Century Amazonian drought risk. *Earth's Future* **8**, e2020EF001608 (2020), 10.1029/2020EF001608.
25. J. P. Dunne *et al.*, The GFDL earth system model version 4.1 (GFDL-ESM 4.1): Overall coupled model description and simulation characteristics. *J. Adv. Model. Earth Syst.* **12**, e2019MS002015 (2020), 10.1029/2019MS002015.
26. V. Eyring *et al.*, Overview of the coupled model intercomparison project phase 6 (CMIP6) experimental design and organization. *Geosci. Model Dev.* **9**, 1937–1958 (2016), 10.5194/gmd-9-1937-2016.
27. I. Martínez Cano *et al.*, Allometric constraints and competition enable the simulation of size structure and carbon fluxes in a dynamic vegetation model of tropical forests (LM3PPA-TV). *Global Change Biol.* **26**, 4478–4494 (2020), 10.1111/gcb.15188.
28. S. S. Rabin *et al.*, A fire model with distinct crop, pasture, and non-agricultural burning: Use of new data and a model-fitting algorithm for FINAL.1. *Geosci. Model Dev.* **11**, 815–842 (2018), 10.5194/gmd-11-815-2018.
29. D. S. Ward, E. Shevliakova, S. Malyshev, S. Rabin, Trends and variability of global fire emissions due to historical anthropogenic activities. *Global Biogeochem. Cycles* **32**, 122–142 (2018), 10.1002/2017GB005787.
30. B. C. O'Neill *et al.*, The scenario model intercomparison project (ScenarioMIP) for CMIP6. *Geosci. Model Dev.* **9**, 3461–3482 (2016), 10.5194/gmd-9-3461-2016.
31. R. Döscher *et al.*, The EC-Earth3 earth system model for the climate model intercomparison project 6. *Geosci. Model Dev.* **15**, 2973–3020 (2022), 10.5194/gmd-15-2973-2022.
32. R. Ramo *et al.*, African burned area and fire carbon emissions are strongly impacted by small fires undetected by coarse resolution satellite data. *Proc. Natl. Acad. Sci. U.S.A.* **118**, e2011160118 (2021), 10.1073/pnas.
33. M. W. Jones *et al.*, Global and regional trends and drivers of fire under climate change. *Rev. Geophys.* **60**, e2020RG000726 (2022), 10.1029/2020RG000726.
34. Y. Chen *et al.*, Forecasting fire season severity in south america using sea surface temperature anomalies. *Science* **334**, 787–791 (2011), 10.1126/science.1209472.
35. H.-B. Fredriksen, J. Berner, A. C. Subramanian, A. Capotondi, How does El Niño-Southern Oscillation change under global warming–A first look at CMIP6. *Geophys. Res. Lett.* **47**, e2020GL090640 (2020), 10.1029/2020GL090640.
36. W. Cai *et al.*, Changing El Niño-Southern oscillation in a warming climate. *Nat. Rev. Earth Environ.* **2**, 628–644 (2021), 10.1038/s43017-021-00199-z.
37. T. M. Lenton *et al.*, Tipping elements in the Earth's climate system. *Proc. Natl. Acad. Sci. U.S.A.* **105**, 1786 (2008), 10.1073/pnas.0705414105.
38. S. Drijfhout *et al.*, Catalogue of abrupt shifts in intergovernmental panel on climate change climate models. *Proc. Natl. Acad. Sci. U.S.A.* **112**, E5777 (2015), 10.1073/pnas.1511451112.
39. B. Smith *et al.*, Implications of incorporating N cycling and N limitations on primary production in an individual-based dynamic vegetation model. *Biogeosciences* **11**, 2027–2054 (2014), 10.5194/bg-11-2027-2014.
40. P. M. Cox, Emergent constraints on climate-carbon cycle feedbacks. *Curr. Climate Change Rep.* **5**, 275–281 (2019), 10.1007/s40641-019-00141-y.
41. M. Wu, B. Smith, G. Schurgers, A. Ahlström, M. Rummukainen, Vegetation-climate feedbacks enhance spatial heterogeneity of pan-amazonian ecosystem states under climate change. *Geophys. Res. Lett.* **48** e2020GL092001 (2021), 10.1029/2020GL092001.
42. C. H. L. Silva Junior *et al.*, Persistent collapse of biomass in Amazonian forest edges following deforestation leads to unaccounted carbon losses. *Sci. Adv.* **6**, eaaz8360 (2020), 10.1126/sciadv.aaz8360.
43. T. Matricardi Eraldo Aparecido *et al.*, Long-term forest degradation surpasses deforestation in the Brazilian Amazon. *Science* **369**, 1378–1382 (2020), 10.1126/science.abb3021.
44. A. Esquivel-Muelbert *et al.*, Compositional response of Amazon forests to climate change. *Global Change Biol.* **25**, 39–56 (2019), 10.1111/gcb.14413.
45. P. M. Brando *et al.*, Fire-induced tree mortality in a neotropical forest: The roles of bark traits, tree size, wood density and fire behavior. *Global Change Biol.* **18**, 630–641 (2012), 10.1111/j.1365-2486.2011.02533.x.
46. N. Strigul, D. Pristinski, D. Purves, J. Dushoff, S. Pacala, Scaling from trees to forests: Tractable macroscopic equations for forest dynamics. *Ecol. Monogr.* **78**, 523–545 (2008), 10.1890/08-0082.1.
47. E. S. Weng *et al.*, Scaling from individual trees to forests in an Earth system modeling framework using a mathematically tractable model of height-structured competition. *Biogeosciences* **12**, 2655–2694 (2015), 10.5194/bg-12-2655-2015.
48. A. Wolf, W. R. L. Anderegg, S. W. Pacala, Optimal stomatal behavior with competition for water and risk of hydraulic impairment. *Proc. Natl. Acad. Sci. U.S.A.* **113**, E7222–E7230 (2016), 10.1073/pnas.1615144113.
49. S. Evans, P. Ginoux, S. Malyshev, E. Shevliakova, Climate-vegetation interaction and amplification of Australian dust variability. *Geophys. Res. Lett.* **43**, 11,823–11,830 (2016), 10.1002/2016GL071016.
50. S. Evans, S. Malyshev, P. Ginoux, E. Shevliakova, The impacts of the dust radiative effect on vegetation growth in the sahel. *Global Biogeochem. Cycles* **33**, 1582–1593 (2019), 10.1029/2018GB006128.
51. L. Yin, R. Fu, E. Shevliakova, R. E. Dinkinson, How well can CMIP5 simulate precipitation and its controlling processes over tropical South America? *Clim. Dyn.* **41**, 3127–3143 (2013), 10.1007/s00382-012-1582-y.
52. B. Saugier, J. Roy, H. A. Mooney, *Terrestrial Global Productivity*, B. Saugier Roy, H. A. Mooney, Eds. (Academic Press, San Diego, 2001), pp. 543–557.
53. L. Giglio, J. T. Randerson, G. R. van der Werf, Analysis of daily, monthly, and annual burned area using the fourth-generation global fire emissions database (GFED4). *J. Geophys. Res. Biogeosci.* **118**, 317–328 (2013), 10.1002/jgrg.20042.
54. G. R. van der Werf *et al.*, Global fire emissions estimates during 1997–2016. *Earth Syst. Sci. Data* **9**, 697–720 (2017), 10.5194/essd-9-697-2017.
55. G. J. van Oldenborgh, L. A. te Raa, H. A. Dijkstra, S. Y. Philip, Frequency- or amplitude-dependent effects of the Atlantic meridional overturning on the tropical Pacific Ocean. *Ocean Sci.* **5**, 293–301 (2009), 10.5194/os-5-293-2009.
56. V. Avitabile *et al.*, An integrated pan-tropical biomass map using multiple reference datasets. *Global Change Biol.* **22**, 1406–1420 (2016), 10.1111/gcb.13139.